Centrality Dependence of Charged Particle Multiplicity in Au-Au Collisions at $\sqrt{s} = 130$ A GeV

PHENIX Collaboration
(December 9, 2000)

We present results for the charged-particle multiplicity distribution at mid-rapidity in Au - Au collisions at $\sqrt{s} = 130$ A GeV measured with the PHENIX detector at RHIC. For the 5% most central collisions we find $dN_{ch}/d\eta_{|\eta=0} = 622 \pm 1(stat) \pm 41(syst)$. The results, analyzed as a function of centrality, show a steady rise of the particle density per participating nucleon with centrality.

PACS: 25.75.-q, 25.75.Dw

The Relativistic Heavy-Ion Collider (RHIC) at Brookhaven National Laboratory started regular operation in June 2000, opening new frontiers in the study of hadronic matter under unprecedented conditions of temperature and energy density. The research is focussed on the phase transition associated with quark deconfinement and chiral symmetry restoration expected to take place under those conditions.

In this letter, we report results for the charged-particle multiplicity distribution at mid-rapidity in Au - Au collisions at $\sqrt{s} = 130$ A GeV as measured with the PHENIX detector. These are the first results which span a broad impact parameter range.

Particle density at mid-rapidity is an essential global variable for the characterization of nuclear collisions at ultra-relativistic energies, providing information about the initial conditions, such as energy density. The results presented here should help to constrain the wide range of theoretical predictions [1] available at RHIC energies and to discriminate among various mechanisms of entropy and particle production. In particular, we analyze the particle density as a function of centrality, expressed by the number of participating nucleons. Such an analysis may shed light on the relative importance of soft versus hard processes of particle production and test the assumption of gluon saturation expected at RHIC energies [2,3]. Our results are compared to different models, to similar studies obtained in Pb-Pb collisions at the CERN SPS [4–6] and to a recent measurement performed at RHIC by PHOBOS [7].

The PHENIX detector consists of an axial-field magnet with two central arms, the east and west arms, each one subtending 90^o in azimuth (ϕ) and ± 0.35 units of pseudorapidity (η). Two spectrometers, the north and south spectrometers, at forward angles ($10^o < \theta < 35^o$) around the beam axis serve to identify and track muons [8]. The present analysis relies primarily on three PHENIX subsystems: the Zero Degree Calorimeters (ZDC) and the Beam-Beam Counters (BBC), used to derive the trigger and the off-line event selection, and the two layers of Pad Chambers (PC) of the east arm, used to determine the charged particle multiplicity.

The ZDC are small transverse-area hadron calorimeters that measure neutron energy within a 2 mrad ($|\eta| > 6$) cone around the beam direction and are located at ± 18.25m from the center of the interaction region. Each of the experiments at RHIC has an identical pair of ZDC. In PHENIX they serve two roles: they provide a trigger and a measure of centrality since their energy signal is proportional to the number of spectator neutrons [9].

The BBC comprise two arrays of 64 photomultiplier tubes each equipped with quartz Cherenkov radiators. They are located around the beam direction at ± 1.44m from the center of the interaction region covering the full 2π azimuth and the range $\eta = \pm$ (3.0 - 3.9). They provide the start timing and one of the triggers [10].

The pad chambers provide three-dimensional coordinates along the charged-particle trajectories [11]. Each PC layer has 8 wire chambers with cathode pad readout (see Figure 1). In the east arm there are two layers, called PC1 and PC3, placed at radial distances of 2.49 m and 4.98 m, respectively, from the interaction region.

The primary interaction trigger is generated by a coincidence between the north and south BBC with at least two photomultipliers fired in each of them and a requirement on the collision vertex position, usually $|z| \leq 20$ cm. Based on detailed simulations of the BBC, this trigger reflects $[92 \pm 2(syst)]$% of the nuclear interaction cross section of 7.2 barns [12]. Another trigger is generated by a coincidence between the north and south ZDC, each one with an energy signal larger than 10 GeV. This trigger reflects the nuclear interaction plus the mutual Coulomb dissociation cross sections.

For this analysis, the BBC trigger is required but most events (97.8%) also satisfy the ZDC trigger requirement. The small percentage of exclusive BBC triggers has two components. The first one accounts for the sub-percent level inefficiency of the ZDC trigger for very central collisions. The second component is from low-multiplicity events originating from peripheral collisions where the ZDC may have some inefficiency or from background interactions. These two sources are difficult to distinguish and we estimate a background event contamination of $[1 \pm 1(syst)]$% of the total event sample.

The analysis described here is based on a sample of events taken without magnetic field. The sample size is reduced offline by requiring the vertex to be within a distance $z = \pm 17$ cm from the center of the interaction region resulting in a total of 137,784 analyzed events.

The number of primary charged particles per event is determined on a statistical basis by correlating hits in PC1 and PC3, rather than by explicit track reconstruction. The analysis procedure was developed and corroborated by extensive Monte Carlo studies using the GEANT [13] response of the PHENIX detector to events generated with HIJING [14]. We first attempt to reconstruct the vertex from PC1/3 using the following algorithm: all hits in PC3 are combined with all hits in PC1 and the resulting lines are projected onto a plane through the beam line, symmetrically placed with respect to the tracking arms (see Fig. 1). For all events with more than $\sim$5 tracks, the distribution of these projections along the Z axis produces a distinct peak which defines the vertex position. For low-multiplicity events where the number of tracks is too small to allow vertex determination by the PC, the vertex is reconstructed from the time difference between the north and south BBC.

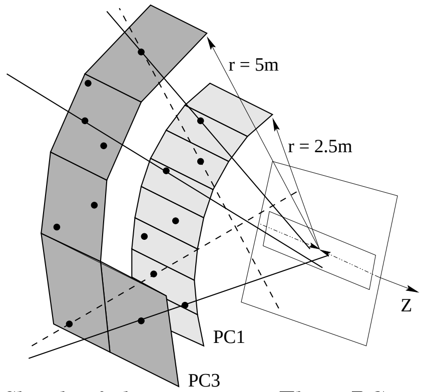

FIG. 1. Sketch of the geometry. Three PC3 sectors have been removed from the drawing in order to show the detail beneath.

Once the vertex is known, the number of tracks is determined from the correlation of hits in PC1 and PC3. All hits in PC3 are again combined with all hits in PC1 and the resulting tracks are projected onto the plane previously defined. The distribution of the distance R of the intersection points to the vertex position, is shown in Fig. 2. Two main classes of tracks contribute to this distribution: real tracks and tracks from the obvious combinatorial background inherent to the adopted procedure of combining all hits in PC3 with all hits in PC1. The latter can be determined by a mixed event technique; in the present analysis, each sector in PC1 was exchanged with its neighbor and the resulting combinatorial background is shown in Fig. 2 by the dotted line. The yield of this background increases quadratically with R (leading to a linear dependence in the differential dN/dR vs. R presentation of Fig. 2).

The R distribution of real tracks (N_R) obtained by subtracting the background (N_B) from the total number of tracks (N_T) is shown in Fig. 2 by the dashed line. The

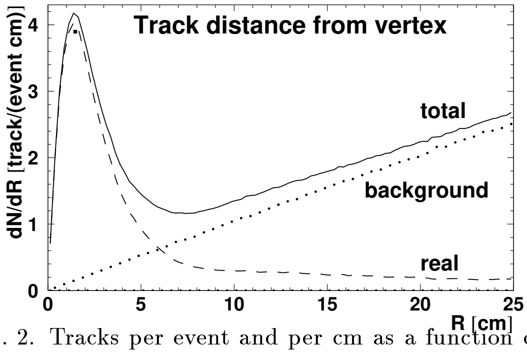

FIG. 2. Tracks per event and per cm as a function of the distance to the event vertex.

sharp peak at small R is due to tracks from primary particles originating at the vertex and the long tail is due to decay products of primary particles decaying in flight. In practice, the track counting is performed up to a given R value. The fraction of counted tracks as a function of R is obtained from the integral of the dashed curve normalized to the total integral up to $R = \infty$. The tail due to decays at large R values is very well described by an exponential function and therefore the extrapolation of the dashed curve to $R = \infty$ is straightforward. The larger the value of R, the smaller is the correction for the fraction of uncounted tracks but the larger the background to be subtracted. Since the background can be reliably subtracted we performed the track counting up to R=25cm, thus including 95.9% of all tracks.

After subtracting the background, a raw multiplicity distribution is obtained to which several correction factors are applied to obtain a fully corrected multiplicity distribution of primary charged particles:
i) A correction of 15.3% accounts for inactive gaps between the chambers, inactive electronic readout cards and dead pads in the PC1 and PC3 detectors.
ii) Using cosmic rays, the pad chamber intrinsic hit efficiency was measured to be 99.4% for isolated single hits in agreement with an analytical study of the pad chamber performance [15].
iii) The track losses due to the finite double hit resolution of the chambers depend on the event multiplicity. The losses are due to two effects, in the direct counting of tracks and in the subtraction of the combinatorial background by event mixing. The two effects were studied in great detail with Monte Carlo techniques. For the first one, the correction amounts to 13.3% for the 5% most central collisions, whereas it is only 4.9% for the 20-25% bin. The second effect is a reduction of the combinatorial background which leads to an increase in the track multiplicity by $0.036 \times N_B$.
iv) Finally there is a correction due to uncounted charged tracks. Two sources contribute here. First, tracks are missed because the analysis is limited to R=25cm. As discussed above, this correction is determined from Fig. 2 and amounts to 4.3%. The second source has two components. On the one hand there are primary charged parti-

cles (mainly $\pi^{\pm}$) which decay in flight. A large fraction of these decays are accounted for since, as discussed above, they produce the tail of the R distribution in Fig. 2. However, there is still a small number of decays which miss altogether PC1 and/or PC3 and those have to be added. On the other hand, there is feed-down from neutral particle decays (mainly K_S^o and π^o) which lead to valid tracks. Those have to be subtracted. Both components depend on particle composition and momentum distribution. Lacking precise information about them, we performed Monte Carlo simulations, applying to the GEANT response of the pad chambers the same analysis procedure as to the real data and comparing the resulting multiplicity to the original HIJING input. The result is a net correction of only ~2.8%. This correction is quite robust against changes in the input. For example, a uniform 20% increase in the momentum p of all pions reduces the net correction to 1%.

The systematic error in the multiplicity due to corrections i) and ii) is estimated at less than 2%. To these we have to add the systematic uncertainties of the analysis procedure, mainly those associated with the background subtraction, double hit resolution (which are multiplicity dependent) and particle decays (which is multiplicity independent). We estimate the first two uncertainties to be 4.6% at the highest multiplicities, based on Monte Carlo guidance and a comparison with an identical analysis in which we imposed a 50% larger double hit resolution in both PC1 and PC3. For the correction for particle decays, we assign a systematic error of 4% based on the effect of varying the momentum distribution and the particle composition in the simulations and a comparison with the results obtained with another data set measured while the east arm was retracted by 44 cm from its nominal position. Adding these errors in quadrature results in a total systematic error of 6.5% at the highest multiplicities. An additional error in $dN_{ch}/d\eta$, which enters in the analysis of the multiplicity versus centrality presented below, is the uncertainty in the total number of events resulting from the BBC trigger efficiency (±2%) and the background event contamination (±1%).

After applying the appropriate corrections we obtain in the lower panel of Fig. 3 the minimum-bias charged-particle multiplicity distribution, in the track acceptance of one full central arm of the PHENIX detector ($|\eta| < 0.35$, $\delta\phi = 88.4^o$). A factor of 5.82 thus converts the observed number of tracks to $dN_{ch}/d\eta_{|\eta=0}$ in one unit of pseudo-rapidity and full azimuth, yielding the lower horizontal scale in Fig. 3.

Fig. 3 also shows the multiplicity distributions for the four most central bins, 0-5% to 15-20%. The bins were defined by cuts in the space of BBC versus ZDC analog response (see Fig. 3 - upper panel) and refer to percentiles of the total interaction cross section of 7.2 barns. In order to avoid the ambiguities inherent in the BBC vs. ZDC distribution, we selected events with increasing centrality based upon the monotonic response of the west arm PC1 pad chambers. The centroids of these events projected onto the ZDC-BBC space determine the centrality contour indicated by the solid line. The cuts are made perpendicular to this contour. Simulations of the response of the BBC and the ZDC were used to account for the effect of physics and detector fluctuations in the definition of these event classes and to relate them via a Glauber model [12] to the number of participating nucleons N_p and the number of binary collisions N_c. The average charged particle density scaled up to one unit of rapidity and the corresponding number of participants and collisions are tabulated in Table 1 for various centrality bins.

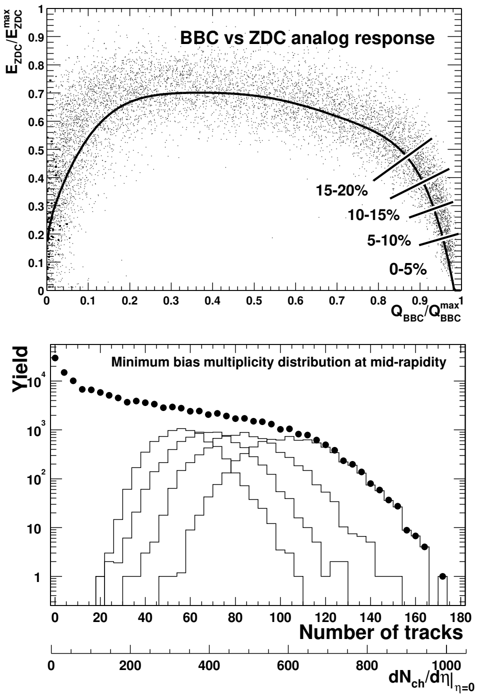

FIG. 3. BBC vs. ZDC analog response (top panel) and minimum-bias multiplicity distribution (lower panel)

TABLE I. Charged-particle density, number of participating nucleons and number of collisions for various centrality bins. The statistical errors are negligible and only systematic errors are quoted.

Percentile of σ_{geo}=(7.2 b)	$< dN_{ch}/d\eta_{|\eta=0} >$	$< N_p >$	$< N_c >$
0 - 5	622 ± 41	347 ± 10	946 ± 146
5 - 10	498 ± 31	293 ± 9	749 ± 116
10 - 15	413 ± 25	248 ± 8	596 ± 93
15 - 20	344 ± 21	211 ± 7	478 ± 75
20 - 25	287 ± 18	177 ± 7	377 ± 61
25 - 30	235 ± 16	146 ± 6	290 ± 47
30 - 35	188 ± 14	122 ± 5	226 ± 38
35 - 40	147 ± 12	99 ± 5	170 ± 30
40 - 45	115 ± 11	82 ± 5	130 ± 24
45 - 50	89 ± 9	68 ± 4	101 ± 19

The PHOBOS experiment has recently reported an average $dN_{ch}/d\eta_{|\eta=0} = 555 \pm 12(stat) \pm 35(syst)$ for the 6% most central collisions [7]. For the same centrality bin, we find $dN_{ch}/d\eta_{|\eta=0} = 609 \pm 1(stat) \pm 37(syst)$. From the preliminary results reported by the NA49 experiment in Pb-Pb collisions at the highest CERN SPS energy of $\sqrt{s}$= 17.2 A GeV, [6], we derive a particle density $dN_{ch}/dy_{|y=0} = 410$. If we scale this result by 0.9 to account for the tranformation to pseudo-rapidity, our result for the same centrality bin (0-5%), is $dN_{ch}/d\eta_{|\eta=0} = 622$, representing an increase of $\sim 60\%$.

It has recently been emphasized [2] that the centrality dependence of $dN_{ch}/d\eta$ allows one to discriminate between various theoretical models of particle production. We show in Fig. 4 our results for $dN_{ch}/d\eta$ per participating nucleon pair as a function of the number of participating nucleons N_p. Fig. 4 also shows the $p\overline{p}$ value at the same $\sqrt{s}$ taken from the UA5 analysis [16]. It is interesting to note that the extrapolation of our data points to low multiplicities approaches the $p\overline{p}$ value.

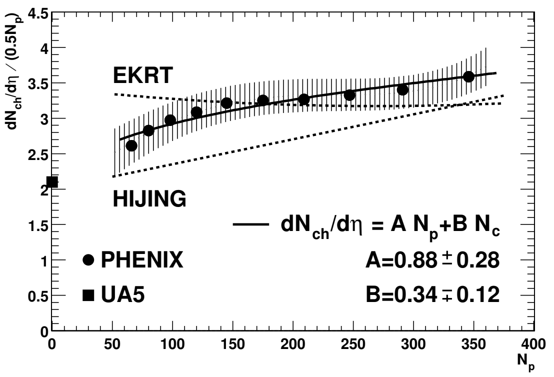

FIG. 4. Charged-particle pseudo-rapidity density per pair of participating nucleons vs. the number of participating nucleons. Predictions from HIJING [2] and EKRT [3] models, and a simple phenomenological fit are also shown. The shaded area represents the systematic errors of $dN_{ch}/d\eta$ and N_p. The errors of N_c are in Table 1.

Models such as HIJING predict that there is a component of particle production from soft interactions that scales linearly with N_p and a second component from hard processes (pQCD jets) that scales with the number of binary collisions N_c. Following that, we fit the data of Fig. 4 with the function:

$$dN_{ch}/d\eta = A \times N_p + B \times N_c$$

using the values of N_c and N_p tabulated in Table 1. The results of the fit are shown in Fig. 4. In the framework of such models, the values of A and B imply a large contribution of hard processes to particle production, which increases with centrality from $\sim 30\%$ at N_p=68 to $\sim 50\%$ for central collisions. HIJING predicts the same trend although the calculated values are lower than the data by $\sim 15\%$.

However, this is not a unique interpretation. At AGS energies, where hard processes do not occur, the particle production per participant was also observed to increase with centrality [17]. At the CERN SPS energy of $\sqrt{s} = 17.2$ A GeV, experiments NA49 [6] and WA98 [4] observed a similar behavior and using a different parametrization, $dN_{ch}/d\eta \propto N_p^{\alpha}$, WA98 finds a best fit value of $\alpha = 1.08 \pm 0.03$. Experiment WA97 quotes a value $\alpha = 1.05 \pm 0.05$, consistent with the result of WA98 but also compatible with their assumption of proportionality between multiplicity and participants [5]. A good fit to our data can also be obtained with this functional form with a higher value of $\alpha = 1.16 \pm 0.04$. One should note that the CERN results are in the lab frame whereas our are in the center of mass system.

Other models such as the EKRT [3] predict that at RHIC energies, the large production of semi-hard gluons in a small volume may saturate the gluon density. The resulting gluon fusion limits the total entropy production and thus lowers the final particle production per participant. The predictions of the EKRT model are also shown in Fig. 4. We observe no such saturation effect within our errors for Au + Au collisions at $\sqrt{s} = 130$ A GeV, but instead see a steady rise in the particle production per participant pair.

We thank the staff of the RHIC project, C-A, and Physics Departments at BNL and the staff of PHENIX participating institutions for their vital contributions. We acknowledge support from the Department of Energy and NSF (U.S.A.), Monbu-sho and STA (Japan), RAS, RMAE, and RMS (Russia), BMBF (Germany), FRN, NFR, and the Wallenberg Foundation (Sweden), MIST and NSERC (Canada), CNPq and FAPESP (Brazil), IN2P3/CNRS (France), DAE (India), KRF and KOSEF (Korea), and the US-Israel Binational Science Foundation.

[1] S.A. Bass et al., Nucl. Phys. **A661**, 205c (1999).
[2] X.N. Wang and M. Gyulassy, nucl-th/0008014.
[3] K.J. Eskola et al. Nucl. Phys. **B570**, 379 (2000) and hep-ph/0009246.
[4] WA98 Collaboration, M.M. Aggarwal et al., nucl-ex/008004.
[5] WA97 and NA57 Collaborations, F. Antinori et al., Preprint CERN-EP-2000-002.
[6] NA49 Collaboration, J. Bachler et al., Nucl. Phys. **A661**, 45c (1999).
[7] PHOBOS Collaboration, B.B. Back et al., Phys. Rev. Lett. **85**, 3100 (2000).
[8] PHENIX Collaboration, D.P. Morrison, Nucl. Phys. **A638**, 565c (1998); *ibid* PHENIX Collaboration, N. Saito, p. 575c.
[9] C. Adler et al., nucl-ex/0008005.
[10] K. Ikematsu et al., Nucl. Instrum. Meth. **A411**, 238 (1998).
[11] P. Nilsson et al., Nucl. Phys. **A661**, 665c (1999) and in preparation.

[12] The cross section was calculated using a Glauber model with a nuclear density described by a Woods-Saxon distribution, a gold nucleus radius R=6.65fm, a diffuseness a=0.54fm and a nucleon-nucleon inelastic cross section σ_{nn}=40mb.
[13] GEANT 3.2.1, CERN program library.
[14] X.N. Wang and M. Gyulassy, Phys. Rev. **D44**, 3501 (1991). We used version 1.35 with default parameters.
[15] A. Milov et al., PHENIX technical note 379.
[16] UA5 Collaboration, G.J. Alner et al., Z. Phys. **C33**, 1 (1986).
[17] E-802 Collaboration, L. Ahle et al., Phys. Rev. **C59**, 2173 (1999).